11 Liquid resin, polymer solution and latex processing

Dr. Chensong Dong

Department of Mechanical Engineering

Curtin University of Technology

GPO Box U1987

Perth, WA 6845

Australia

Email: c.dong@curtin.edu.au

Abstract

This chapter represents a very important aspect of composite manufacturing: the processing of liquid resin, polymer solution, latex and their composites. First, basic material properties including viscosity and curing are introduced. Common techniques for liquid resin and composite processing are then presented. Finally, the issues and problems associated with processing are discussed.
Keywords: liquid; resin; latex; processing

11.1 Introduction

Liquid processing is a complex process involving resin flow, chemical reaction, and heat transfer. The unique properties of polymers play an important role. Several processing techniques including hand lay-up, spray-up, resin casting, resin transfer moulding, and vacuum-assisted resin transfer moulding, etc. are presented. The issues and problems associated with processing are discussed.

11.2 Viscosity of resin

Viscosity is a measure of the resistance of a fluid to flow under shear stresses. It is defined as the ratio of shear stress and shear rate. The viscosity of a fluid is generally dependent on its molecular-weight. Low molecular-weight fluids such as water have low viscosities. High molecular-weight fluids such as polymer melts have high viscosities.

Two important factors determining the viscosity of a fluid are the temperature and shear rate. For all fluids, the viscosity decreases with increasing temperature. Depending on the influence of shear rate, fluids can be classified as Newtonian and non-Newtonian fluids. In Newtonian fluids, the viscosity is independent of the shear rate while in non-Newtonian fluids, the viscosity changes with the shear rate. Non-Newtonian fluids can be further divided into shear thickening and shear thinning fluids, as shown in Figure 1.

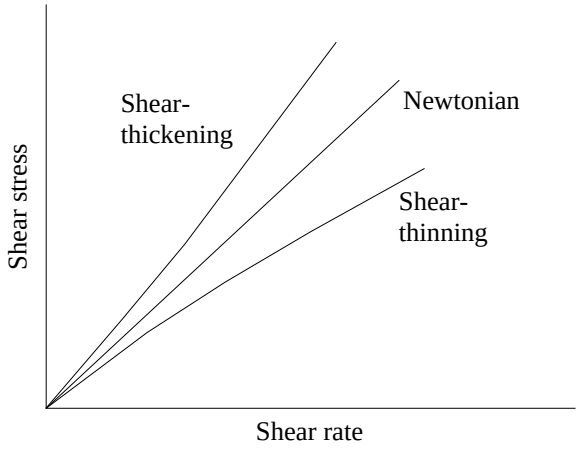

Figure 1: Newtonian and non-Newtonian fluids

The starting material for a thermosetting resin is a low-viscosity fluid. Its viscosity increases with curing and approaches a very high value as it transforms into a solid state. During isothermal curing, the viscosity increases with increasing curing time and temperature. The viscosity change of an epoxy resin system – EPON 862/W with temperature and curing time is shown in Figure 2. After a threshold degree of cure is achieved, the resin viscosity increases at a very rapid rate. The time at which this occurs is called the gel time, which is a very important moulding parameter.

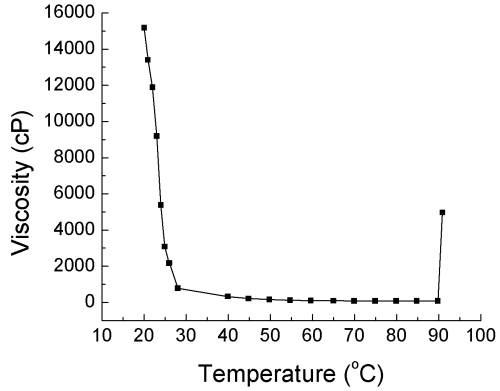

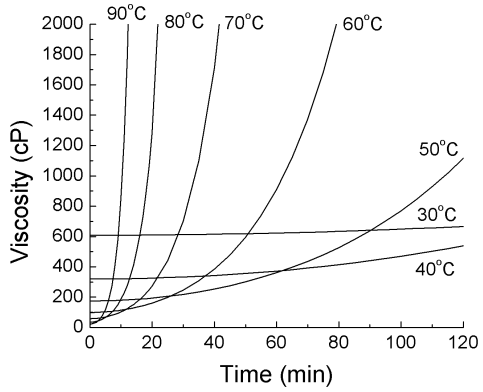

Figure 2: Viscosity vs. temperature and curing time for EPON 862/W

The viscosity of resin η during the curing process is a function of curing temperature T, shear rate $\dot{\gamma}$ and the degree of cure α:

$$\eta = \eta(T, \dot{\gamma}, \alpha) \qquad [11.1]$$

At a constant shear rate and for the same degree of cure, the viscosity is given by

$$\eta = \eta_0 \exp\left(-\frac{\Delta E}{RT}\right) \qquad [11.2]$$

where

η_0 = constant

ΔE = flow activity energy

R = universal gas constant

T = curing temperature (°K)

11.3 Curing

The curing reaction of liquid resin is commonly experimentally investigated by using differential scanning calorimetry (DSC). It can identify and characterize polymerization, cross-linking, crystallization, and fusion (or melting) of crystallites in terms of heat evolved or absorbed and the associated transition temperatures. Furthermore, these thermal data enable one to deduce the reaction rate constant, kinetic reaction order, activation energy, etc. DSC analyses can be made either isothermally as a function of time of dynamically as function of temperature.

In DSC measurements, the degree of cure of conversion can be estimated from the ratio of the amount of heat evolved for the partial conversion after time t at a given temperature, H_t, to the total heat evolved for the complete conversion, H_0, i.e.

$$\alpha = H_t / H_0 \qquad [11.3]$$

The reaction rate is often described by kinetic models. In general, kinetic models may be phenomenological or mechanistic. A phenomenological model captures the main features of the reaction kinetics ignoring the details of how individual species react with each other. Mechanistic models, on the other hand, are obtained from balances of species involved in the reaction; hence, they are better for prediction and interpretation of composition. However, due to the complexity of thermosetting reactions, phenomenological models are the most popular for these systems. Phenomenological models for the reaction rate have the general form (Gonzalez-Romero and Casillas, 1989)

$$\frac{d\alpha}{dt} = Kf(\alpha) \qquad [11.4]$$

where α is the fractional conversion of the reactive group (degree of cure), *t* is the reaction time, *K* is a reaction rate constant, and $f(\alpha)$ represents some function of α. Most commonly, *K* is considered to have an Arrhenius temperature dependence:

$$K = A\exp\left(-\frac{\Delta E}{RT}\right) \qquad [11.5]$$

where *A* is the frequency factor, R is the universal gas constant, ΔE is the activation energy, and *T* is the absolute temperature. As the chemical reaction progresses, the reaction rate decreases. Eventually, the reaction rate approaches zero as the completion of the reaction nears. In the absence of vitrification, the degree of cure will reach unity at the completion of the reaction. With these concepts in mind, a functional form of $f(\alpha)$ is taken as

$$f(\alpha) = (1-\alpha)^n g(\alpha) \qquad [11.6]$$

Combining Equations 11.4-11.6 yields the following general expressions for reaction rate:

$$\frac{d\alpha}{dt} = A\exp\left(-\frac{\Delta E}{RT}\right)(1-\alpha)^n g(\alpha) \qquad [11.7]$$

This equation includes the particular cases of an nth order reaction model with $g(\alpha) = 1$ and the autocatalytic model with $g(\alpha) = 1 + C\alpha$, where *C* is the autocatalysis intensity. In general, the form of $g(\alpha)$ must be determined from experimental data.

Various cure kinetic models for thermosetting resins have been developed by researchers. The curing kinetics of epoxy and polyester systems are given by Kamal et al. (Kamal, 1974, Kamal and Sourour, 1973) as

$$\frac{d\alpha}{dt} = (K_1 + K_2\alpha^m)(1-\alpha)^n \qquad [11.8]$$

where, K_1 and K_2 are Arrhenius rate constants given by Equation 11.5 with appropriate activation energies and frequency factors. Bogetti and Gillespie (Bogetti and Gillespie, 1991) modelled the response of an unsaturated polymer resin as

$$\frac{d\alpha}{dt} = K(1-\alpha)^n \alpha^m \qquad [11.9]$$

Loos and Springer (Lee, 1982, Loos and Springer, 1983) showed that Hercules 3501-6 epoxy resin could be modelled by

$$\frac{d\alpha}{dt} = (K_1 + K_2\alpha)(1-\alpha)(0.47-\alpha) \text{ for } \alpha \le 0.3 \qquad [11.10a]$$

$$\frac{d\alpha}{dt} = K_3(1-\alpha) \text{ for } \alpha > 0.3 \qquad [11.10b]$$

As an example, the curing kinetics for an epoxy resin system EPON 862/W is

$$\frac{d\alpha}{dt} = 398829.16(1-\alpha)\exp\left(-\frac{8479.67}{T}\right) \qquad [11.11]$$

The curing degree vs. time at different temperatures is shown in Figure 3.

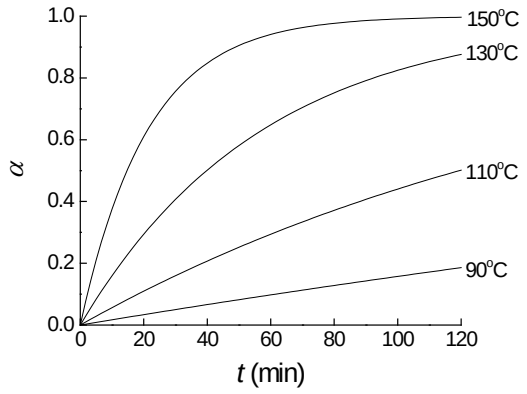

Figure 3: Curing degree vs. time for EPON 862/W

11.4 Liquid resin and composite processing

11.4.1 Hand lay-up

Hand lay-up, the simplest fabrication process, is an open mould process. In hand lay-up, the mould, which is usually made of reinforced plastic, defines the shape of the outer surface. As shown in Figure 4, the mould is first coated with a wax to ensure removal after curing. A layer of gel coat is then sprayed on to the mould to form the outermost surface of the products. The gel coat is allowed to cure for several hours but remains tacky so subsequent resin layers adhere better. Alternate layers of catalysed polyester resin and reinforcement material are applied. The ratio of resin to glass is usually 60 to 40 by weight, but varies by product. Each reinforcement layer is ‘wetted out’ with resin, and then rolled out to remove air pockets. The process continues until the desired thickness is achieved. Hand lay-up is a room temperature curing process.

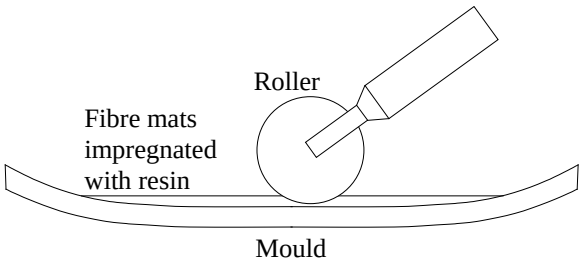

Figure 4: Hand lay-up process

11.4.2 Spray-up

Spray-up is another open-moulding composites fabrication process that uses mechanical spraying and chopping equipment for depositing the resin and glass reinforcement, as show in Figure 5. Resin and chopped glass can be deposited simultaneously or separately to the desired layer thickness on the mould surface (or

on the gel coat that was applied to the mould). This process allows a greater production rate and more uniform parts than does hand lay-up, and often uses more complex moulds.

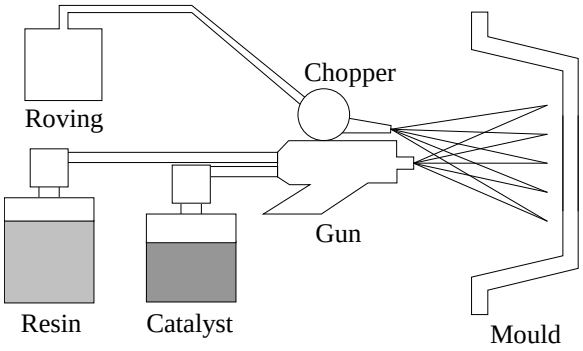

Figure 5: Spray-up process

This process involves the same initial steps (up through application of the gel coat) as used in hand lay-up. Following gel coat application, the polyester resin is applied with a spray gun that has a glass chopper attachment. Layers are built up and rolled out on the mould as necessary to form the part. The spray gun has separate resin and catalyst streams which mix as they exit the gun. However, compared to hand lay-up, more resin is typically used to produce similar parts by spray lay-up because of the inevitable over spray of resin during application.

Resin spray-up is commonly used in open moulding processes in the fibre-reinforced plastics/composites (FRP/C) and boat building industries. Spray-up is also a room temperature curing process.

11.4.3 Resin casting

In the resin casting process, the resin and catalyst are mixed and poured in to various types of moulds at or near room temperatures. The part is cured through chemical reaction and usually with the addition of heat, as shown in Figure 6.

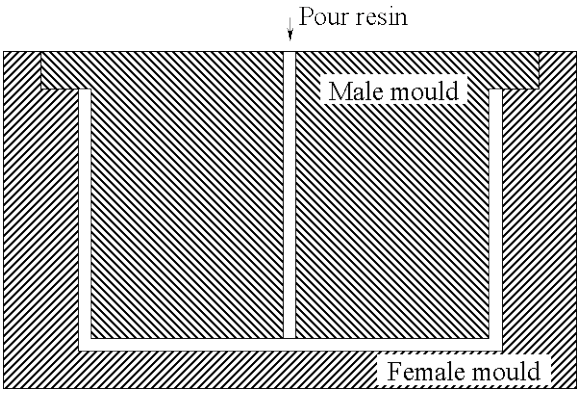

Figure 6: Resin casting

Commonly used materials include epoxies, polyurethanes, and silicones. The moulds can be made of silicone, metal, or epoxy/polyurethane.

11.4.4 Resin transfer moulding

Because of its relatively low equipment and tooling costs, short cycle times and excellent design flexibility, closed-mould liquid composite moulding (LCM) processes which include resin transfer moulding (RTM) and vacuum assisted resin transfer moulding (VARTM) processes are replacing open-mould processes such as hand lay-up and spray-up. The RTM process can be generally divided into four steps as shown in Figure 7 (Gotowsky, 1997). In the first step, dry reinforcements are cut and/or shaped into preformed pieces and then placed in a prepared mould cavity. This is usually called preform loading. After the mould is closed and clamped tightly, resin is injected into the mould cavity, where it flows through the reinforcement preform,

expels the air in the cavity, and ‘wets out’ or impregnates the reinforcement. This step, which is considered the most critical in the RTM process, is called mould filling. When excessive resin begins to flow out of the vent area of the mould, resin injection is stopped and the curing step begins. Curing can take from several minutes to several hours. When curing is complete, the component is removed from the mould. This final step is called demoulding.

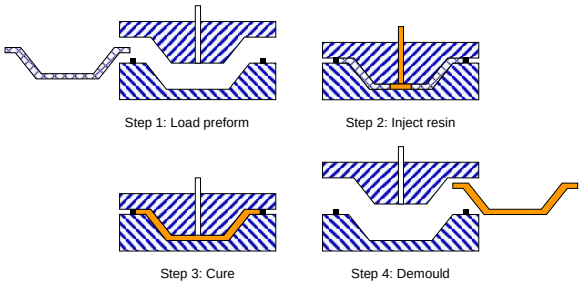

Figure 7: Resin transfer moulding process

11.4.5 VARTM

Vacuum-assisted resin transfer moulding (VARTM) refers to a variety of related processes, which represent the fastest growing new moulding technology. VARTM-type processes and standard RTM differ in that VARTM draws resin into a preform through use of a vacuum, rather than positive pressure. The primary advantage of VARTM is that it does not require high heat or pressure. For this reason, VARTM operates with low-cost tooling, making it possible to inexpensively produce large, complex parts in one shot. This has a great potential for the aerospace industry. Conventional composite parts for commercial aircrafts are fabricated by autoclave process with unidirectional carbon fibre prepreg. Because an autoclave is required to cure the materials, the parts are very expensive (Takeda et al., 2005).

In the VARTM process, as shown in Figure 8, only one rigid mould piece is used and the other mould piece is a vacuum bag. A highly permeable distribution medium is incorporated into preform as a surface layer. During infusion, the resin flows preferentially across the surface and simultaneously through the perform thickness enabling large parts to be fabricated. Current applications include marine, ground transportation and infrastructure parts.

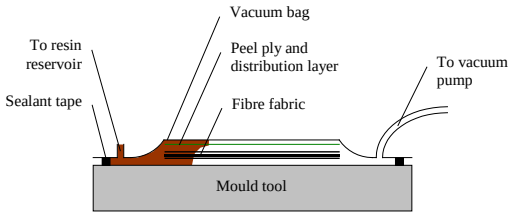

Figure 8: VARTM process

11.4.6 Other liquid resin processing methods

Other liquid resin processing methods include resin injection moulding (RIM), resin film infusion, etc (Gotowsky, 1997). In resin injection moulding process, a rapid-cure resin and a catalyst are injected into the mould in two separate streams; mixing and the resultant chemical reaction both occur in the mould instead of in the dispensing head. The automotive industry is increasingly combining structural RIM (SRIM) with rapid preforming methods to fabricate structural parts that do not require a Class A finish. In resin film infusion process, dry fabrics are laid up interleaved with layers of semi-solid resin film supplied on a release paper. The lay-up is vacuum bagged to remove air through the dry fabrics, and then heated to allow the resin to first melt and flow into the air-free fabrics, and then after a certain time, to cure.

11.5 Resin flow and defect generation

11.5.1 Flow of resin in porous materials

The flow of resin in porous materials is described by Darcy's law as

$$\begin{Bmatrix} u \\ v \\ w \end{Bmatrix} = -\frac{1}{\mu}\begin{bmatrix} k_{xx} & k_{xy} & k_{xz} \\ k_{yx} & k_{yy} & k_{yz} \\ k_{zx} & k_{zy} & k_{zz} \end{bmatrix}\begin{Bmatrix} \frac{\partial p}{\partial x} \\ \frac{\partial p}{\partial y} \\ \frac{\partial p}{\partial z} \end{Bmatrix} \qquad [11.12]$$

where u, v, and w are the velocity components in the x, y, and z directions, respectively. p is the fluid pressure, μ is the viscosity, and the k_{ij}'s are the components of the permeability tensor. Equation 11.12 assumes Newtonian flow. Since the Reynolds number is usually much smaller than one (Tucker, 1993), resin flow can be regarded as Newtonian flow.

The velocity is the apparent fluid velocity which is the product of the actual fluid velocity and ϕ, the porosity of the fibre reinforcement. The porosity is related to the fibre volume fraction v_f as

$$\phi = 1 - v_f \qquad [11.13]$$

The permeability tensor in Equation 11.12 is symmetrical can be diagonalised by coordinate transformation so that

$$\begin{bmatrix} k_{xx} & k_{xy} & k_{xz} \\ k_{yx} & k_{yy} & k_{yz} \\ k_{zx} & k_{zy} & k_{zz} \end{bmatrix} = \mathbf{T}\begin{bmatrix} k_{11} & 0 & 0 \\ 0 & k_{22} & 0 \\ 0 & 0 & k_{33} \end{bmatrix}\mathbf{T}^{\mathbf{T}} \qquad [11.14]$$

where k_{ii}'s are the permeability in the principal directions, and **T** is the transformation matrix. **T** is given by

$$\mathbf{T} = \begin{bmatrix} l_{11} & l_{12} & l_{13} \\ l_{21} & l_{22} & l_{23} \\ l_{31} & l_{32} & l_{33} \end{bmatrix} \qquad [11.15]$$

where l_{ij}'s are the direction cosines of unit vector *i*, with reference to Figure 9.

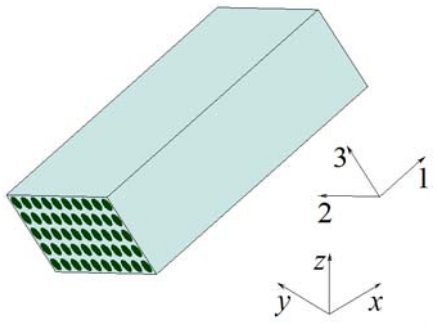

Figure 9: Principal directions vs. global coordinate system

Equation 11.14 can be expanded as

$$\begin{bmatrix} k_{xx} & k_{xy} & k_{xz} \\ k_{yx} & k_{yy} & k_{yz} \\ k_{zx} & k_{zy} & k_{zz} \end{bmatrix} = \begin{bmatrix} l_{11}^2 k_{11} + l_{12}^2 k_{22} + l_{13}^2 k_{33} & l_{11} l_{21} k_{11} + l_{12} l_{22} k_{22} + l_{13} l_{23} k_{33} & l_{11} l_{31} k_{11} + l_{12} l_{32} k_{22} + l_{13} l_{33} k_{33} \\ l_{11} l_{21} k_{11} + l_{12} l_{22} k_{22} + l_{13} l_{23} k_{33} & l_{21}^2 k_{11} + l_{22}^2 k_{22} + l_{23}^2 k_{33} & l_{21} l_{31} k_{11} + l_{22} l_{32} k_{22} + l_{23} l_{33} k_{33} \\ l_{11} l_{31} k_{11} + l_{12} l_{32} k_{22} + l_{13} l_{33} k_{33} & l_{21} l_{31} k_{11} + l_{22} l_{32} k_{22} + l_{23} l_{33} k_{33} & l_{31}^2 k_{11} + l_{32}^2 k_{22} + l_{33}^2 k_{33} \end{bmatrix}$$

[11.16]

Because composite parts are often thin relative to its size and the velocities can be assumed to be constant in the thickness direction. In such case, Equation 11.16 is reduced to

$$\begin{bmatrix} k_{xx} & k_{xy} \\ k_{yx} & k_{yy} \end{bmatrix} = \begin{bmatrix} l_{11}^2 k_{11} + l_{12}^2 k_{22} & l_{11} l_{21} k_{11} + l_{12} l_{22} k_{22} \\ l_{11} l_{21} k_{11} + l_{12} l_{22} k_{22} & l_{21}^2 k_{11} + l_{22}^2 k_{22} \end{bmatrix} \qquad [11.17]$$

As shown in Figure 10, $l_{11} = \cos\theta$, $l_{12} = \sin\theta$, $l_{21} = -\sin\theta$, and $l_{22} = \cos\theta$. Thus,

$$k_{xx} = \frac{k_{11} + k_{22}}{2} + \frac{k_{11} - k_{22}}{2}\cos 2\theta$$
$$k_{xy} = k_{yx} = \frac{k_{11} - k_{22}}{2}\sin 2\theta \qquad [11.18]$$
$$k_{yy} = \frac{k_{11} + k_{22}}{2} - \frac{k_{11} - k_{22}}{2}\cos 2\theta$$

where is the angle between the principal direction 1 and the *x*-axis.

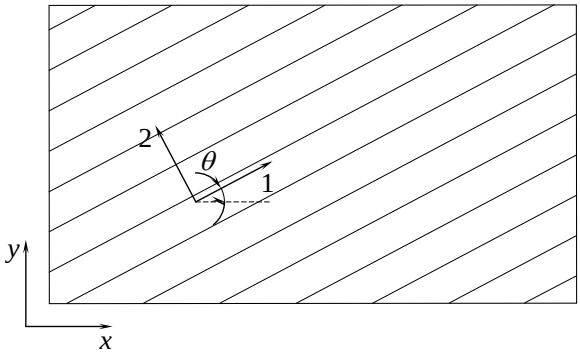

Figure 10: Principal directions vs. coordinate system

When the thickness of the composite part is neglected and the resin flow is considered in 2-D, resin flow can be classified as channel flow and radial flow.

A typical channel flow is shown in Figure 11. In 1-D, the Darcy's law is written as

$$u = -\frac{k}{\mu}\frac{dp}{dx} \qquad [11.19]$$

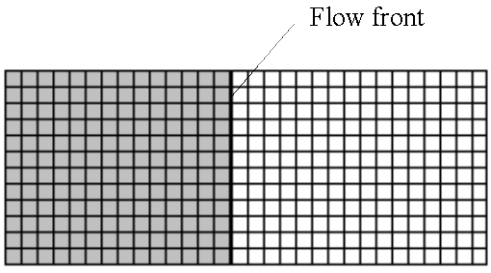

Figure 11: Channel flow apparatus for measuring preform permeability

The closed-form solution for the mould filling time is given by (Cai, 1992a, Cai, 1992b) as

$$t_{fill} = \frac{\phi \mu l^2}{2k\Delta p} \qquad [11.20]$$

where l is the distance from the injection gate to the flow front and Δp is the pressure difference between the injection gate and the flow front.

In a radial flow, resin is injected from the centre of the preform. For an isotropic preform, $k_{11} = k_{22}$, and the flow front will be circular and the fluids moves in the radial direction. The closed-form solution is given by Adams *et al*. (Adams *et al*., 1988) as

$$t_{fill} = \frac{\phi \mu}{4k\Delta p}\left[R_f^2 \ln\left(\frac{R_f^2}{R_0^2}\right) - R_f^2 + R_0^2 \right] \qquad [11.21]$$

For an orthotropic preform, $k_{11} \neq k_{22}$, and the flow front will be ellipse. Figure 12 shows the resin flow fronts of different fibre preforms.

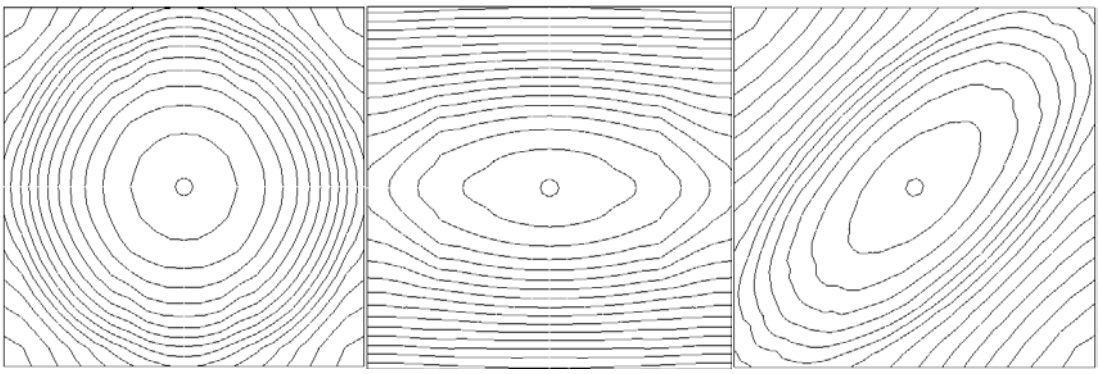

Figure 12: Radial flow in fibre preforms: a) isotropic preform; b) orthotropic preform; and c) orthotropic preform aligned at 45°.

The permeability of fibre preforms can be measured using either channel flow or radial flow. In each case, measurement can be based on either saturated flow measurements or monitoring the progression of the flow front.

11.5.2 Effect of preform deformation

The first type of deformation takes place during the performing stage where fibre fabric is made to conform to the shape of a complex mould. Fibre orientations after deformation are significantly different than those of original fabric and the fibre volume fraction also changes. The dominant mode of in-plane deformation for fibre fabric is shear deformation.

The second type of deformation is the compaction of fibre preforms when the mould is closed. Gutowski et al. (Gutowski et al., 1986) developed a model to predict the relationship between the applied pressure and the fibre volume fraction. Other investigators (Robitaille and Gauvin, 1999, Rudd et al., 1993, Trevino et al., 1991) proposed empirical models. Resin rich areas are usually caused by fibre preform distortion due to compaction of fibre preform and resin infusion. Holmberg and Berglund (Holmberg and Berglund, 1997) studied the manufacturing and performance of RTM U-beams. As the mould closes, the reinforcement tends to pull tight around corners and leaves a resin rich area, as shown in Figure 13.

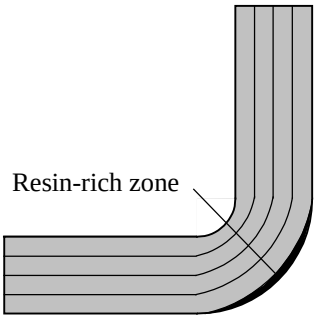

Figure 13: Formation of a resin-rich zone

The third type of deformation occurs near the flow front where the reinforcement is being compressed by the pressure of the advancing resin. Some studies are the work of Gong (Gong, 1993), Farina and Preziosi (Farina and Preziosi, 2000), and Ambrosi and Preziosi (Ambrosi and Preziosi, 1998).

The fourth type of deformation is induced by the resin flow near the inlet, as shown in Figure 14, where three regions can be distinguished: a fibre free region, a saturated fibre bed, and an unsaturated fibre bed. The deformation of the preform away from the wall opens a new channel flow.

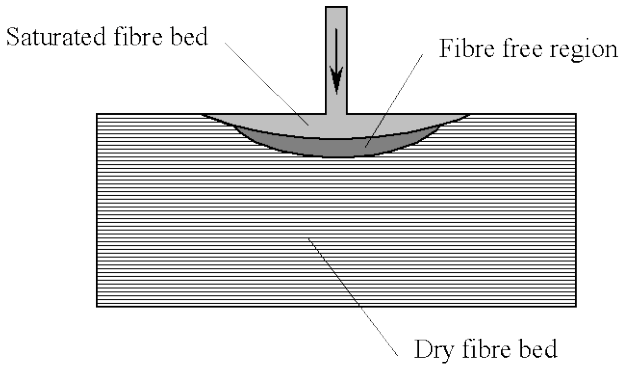

Figure 14: Deformation of fibre preform due to inlet pressure

11.5.3 Dry spots

Voids can be caused by a number of factors. Dry spots or macro-voids are cause by edge flow (race-tracking) and improper vent locations. When the fibre preform is loaded into the mould, it is impossible to obtain a perfect fit, and there will be gaps between the fibre preform and the edge of the mould. The resin will flow faster along the gap because of less resistance. This phenomenon is often called ‘race tracking’ and likely causes dry spots, as shown in Figure 15.

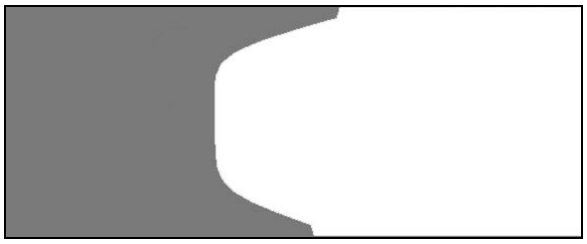

Figure 15: Race tracking

Voids can also be caused by the compression of reinforcement, as illustrated in Figure 16 (Holmberg and Berglund, 1997). At the inner radius the reinforcement is compressed and results in a reduced permeability. The low permeability makes fibre wet-out difficult and an air pocket or void region may form. These can often be eliminated by mould optimisation or control (Jiang et al., 2002, Liu et al., 1996, Trochu et al., 2006).

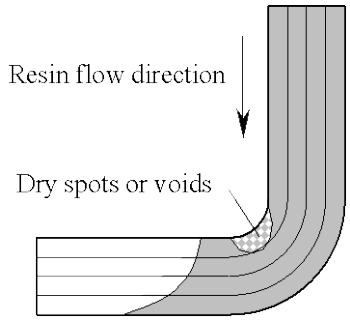

Figure 16: Dry spots or voids caused by the compression of reinforcement

11.5.4 Voids

On a much smaller scale, microvoids are also formed because the heterogeneous nature of fabric reinforcement leads to non-uniform flows and the formation of micro-voids. These voids reduce the strength of the material and should be eliminated. Several studies have been carried out to understand the basic mechanisms of micro-void formation and its governing parameters (Chang and Hourng, 1998, Hamidi, 2004, Kang, 2000, Parnas et al., 1994, Patel, 1995, Patel and Lee, 1995, Rohatgi et al., 1996). The mechanism can be summarized as that the resin near flow front flows at different speeds depending on the microstructure of the reinforcement and air is trapped by the transverse flow. Patel and Lee (Patel and Lee, 1995) show that fibre preforms contain two distinguishable pore structures: micro-pores consisting of gaps between fibre filaments inside fibre tows and macro-pores consisting of much larger gaps between tows. There are several ways in which the competing macro and micro flows can cause microvoids. One example is during transverse flow through an array of fibre bundles air is trapped inside due to the higher flow resistance, as shown in Figure 17 (Kang, 2000, Parnas et al., 1994). Microvoids can also occur when resin flows in the fibre direction. The micro-flow front is ahead of the macro-flow front because of the capillary action, which is often called fingering. If the fibre bundles have transverse stitches, when the flow front reaches the stitches, a flow perpendicular to the fibre direction develops and air is trapped between the fibre bundles, as shown in Figure 18 (Chang and Hourng, 1998, Patel, 1995, Rohatgi et al., 1996).

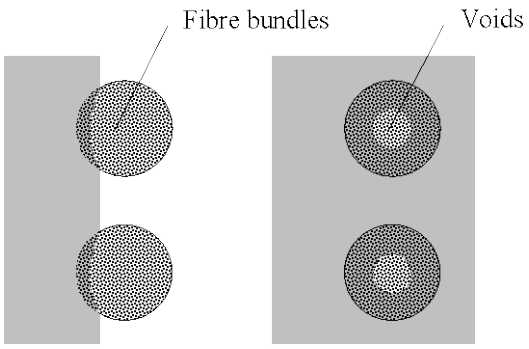

Figure 17: Micro-void formation during flow in the transverse direction

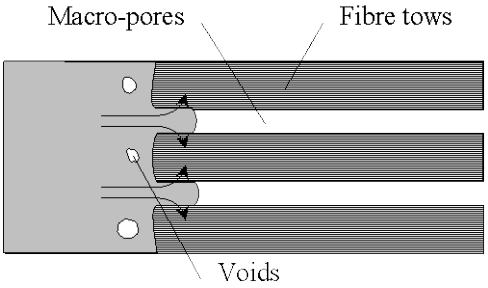

Figure 18: Micro-void formation during flow in the fibre direction

11.6 Dimensional variations

Unlike metals, which can be carved, bent, or stamped into the desired shape, for composites, the material forms as the part forms. The constituent materials of a composite react differently to the changes in environmental conditions encountered during processing. Chemically, the reinforcing fibres do not experience significant change during the process cycle. The thermoset polymer matrix on the other hand contracts during crosslinking by as much as 6% (Yates et al., 1979).

The shrinkage vs. time curves for two epoxy resins cured at 120°C are shown in Figure 19 (Luck and Sadhir, 1992). One very important observation made from these curves is that approximately 60% of the total shrinkage occurs prior to the gel point.

Even though the epoxy resins shrinkage about 4% when fully cured, only about 40% of this shrinkage (1.6%) will occur after gellation to produce internal stresses.

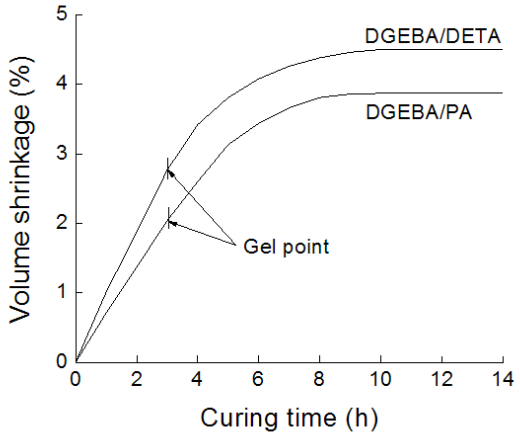

Figure 19: Shrinkage vs. time curves for two epoxy resins at 120°C

As well as chemically-induced deformations, there are thermally-induced deformations during processing. The reinforcing fibres show very little thermal deformation during cool-down along the axis of the fibre. On the other hand, the polymer matrix has a higher thermal expansion coefficient, typically an order of magnitude or more. Because the constituent materials of composites must be well-bonded and uniformly deform to maintain the continuum after processing, these deformations are balanced internally within the composite and residual stresses are induced.

Based on these analyses, it is concluded that the factors causing dimension variations include the volumetric shrinkage of the resin during curing, the mismatch in the coefficients of thermal expansion of the matrix and the fibre. Other factors include tool/part interaction and processing defects.

Due to the anisotropic nature of fibre reinforced materials, the mechanical properties and coefficients of thermal expansion are fibre orientation sensitive. Thus, stacking sequence is a significant factor affecting dimension variations. For asymmetric stacking sequences, the residual stresses are not balanced along the thickness direction and moments of force are induced. These moments of force can cause large warpage such as a ‘saddle’ shape, as shown in Figures 20.

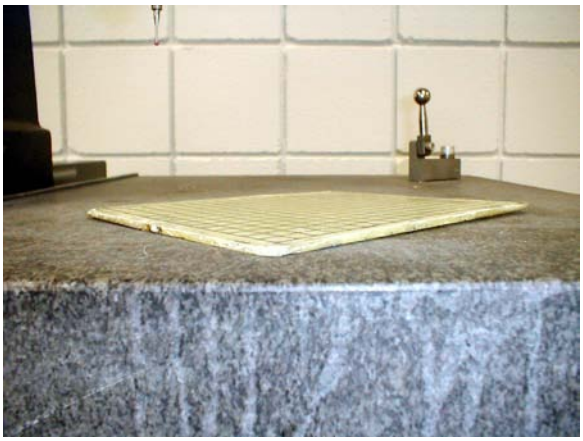

Figure 20: Warpage of a [0/90/0/90/±45/±45/0/90/0/90] E-glass/epoxy panel

For symmetric laminates, the residual stresses are balanced along the thickness direction and deformations are mostly due to the difference of CTE in the in-plane direction and the through-thickness direction. For example, for an angled composite part as shown in Figure 21(a), the CTE in the through-thickness direction is much larger than that in the in-plane direction. Thus, a decreased angle ($\phi' < \phi$) is observed as shown in Figure 21(b), which is commonly called ‘spring-in.’

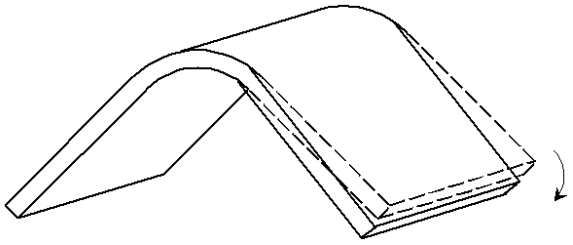

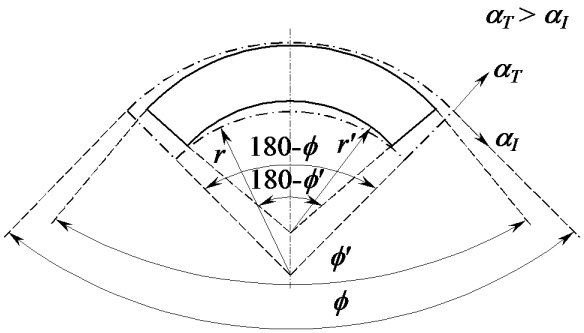

Figure 21: Spring-in of an angled composite part

The closed-form solution for 'spring-in' can be derived as follows. As shown in Figure 21, the included angle is $180-\phi$ and the arc length is $s = r(180-\phi)$. When the temperature is decreases by ΔT, the arc length changes to

$$s' = r(180-\phi)(1+\alpha_I \Delta T);$$

and the radius becomes

$$r' = r(1+\alpha_T \Delta T)$$

The included angle after 'spring-in' is

$$180-\phi' = \frac{s'}{r'} = (180-\phi)\frac{1+\alpha_I \Delta T}{1+\alpha_T \Delta T}$$

Hence, the 'spring-in' is

$$\Delta\phi = \phi' - \phi = \frac{s}{r} - \frac{s'}{r'} = 180 - \phi - (180-\phi)\frac{1+\alpha_I \Delta T}{1+\alpha_T \Delta T}$$

i.e.

$$\Delta\phi = (180-\phi)\frac{(\alpha_T - \alpha_I)\Delta T}{1+\alpha_T \Delta T} \qquad [11.22]$$

Since $1+\alpha_T \Delta T \approx 1$, Equation 11.22 can be reduced to

$$\Delta\phi = (180-\phi)(\alpha_T - \alpha_I)\Delta T \qquad [11.23]$$

The dimensional variation induced in the curing process can be reduced by stress relaxation during the post-curing process. This is illustrated using the spring-in (Svanberg and Holmberg, 2001). As shown in Figure 22, further curing of the resin takes place during the post-curing cycle. During heating to the post-cure temperature, the part will expand and result in a decrease in spring-in angle. At the glass transition temperature (T_g), the resin will change from a glassy to a rubbery state. Any frozen residual stress will be released and results in an increase in spring-in. At temperatures higher that T_g, the CTE of the resin in the rubbery state is much larger than in the glassy state. Therefore, the spring-in angle will decrease at a higher rate. At the post-cure temperature, further cure of the resin will induce chemical curing shrinkage that increases the spring-in. Finally, during cool down, the spring-in will increase to its final value.

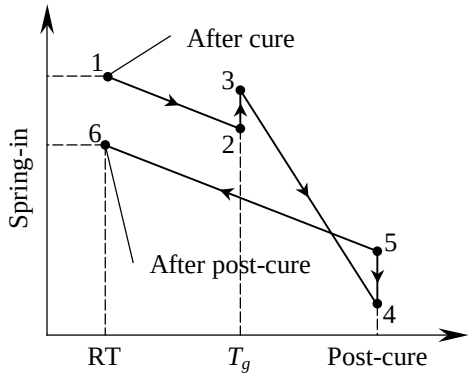

Figure 22: Dimensional variation during post-curing process

The deformations of composites such as warpage and spring-in increase the secondary machining requirements and cost. They also cause matrix micro cracks, and thus weaken the mechanical properties. The deformations often increase the difficulty for the assembly process of composite components. Thus, effective dimension control is

highly desirable to improve the part quality, reduce the cost, and ensure the tolerance requirements for assembly.

Two approaches are mainly used to minimise the dimensional variations in composites processing. The first approach is deformation compensation, where the moulds are modified to account for the dimensional variations generated due to processing. The second method is design optimisation. The design variables such as thickness, curvature radius, stacking sequence, etc. can be varied within some range to minimise the induced dimensional variation.

A special type of dimensional variation occurs in the VARTM process. Typically, thickness gradients and variations result from the infusion pressure gradient during process and material variations. Pressure gradient is the driving force for resin flow and the main source of thickness variation. After infusion, an amount of pressure gradient is frozen into the preform, which primarily contributes to the thickness variation (Li et al., 2006). Studies have shown that debulking can be used to eliminate the part-to-part dimensional variation and quality difference (Robitaille and Gauvin, 1998, Robitaille and Gauvin, 1999). Gama et al. investigated two processing options to improve the dimensional tolerances during VARTM processing. The influence of vacuum debulking on final part has been studied. However, vacuum debulking cannot eliminate the thickness gradient along the infusion direction of the part. Gama et al. (Gama et al., 2001) compared several processing scenarios including ‘Open-Open’, ‘Close-Open’, and ‘Closed-Micro-Flow’. The ‘Close-Open’ processing scenario provides superior compaction and dimensional tolerance over ‘Open-Open’ scenario. One major disadvantage of the ‘Close-Open’ approach is that significant resin

starvation may occur that reduces mechanical properties. The ‘Closed-Micro-Flow’ processing scenario is a new approach that has reduced the thickness gradient in a VARTM part while retaining better mechanical properties as compared to the ‘Open-Open’ processing scenario.

11.7 Future trends

With the stringent requirement of environmental protection, closed-mould processes are replacing open-mould processes. Closed-mould processes including RTM and VARTM offer many advantages including flexibility and low cost. Future work will be focused on the improvement of materials and processes, especially for the aerospace industry. Computer tools including CAD/CAE/CAM will be employed to reduce the cost. Better process control will be applied to reduce the part-to-part variation and improve the quality.

Suggested further reading

Gotowsky, T. G. (1997) *Advanced Composite Manufacturing*, John Wiley & Sons.

Åström, B. T. (1997) *Manufacturing of Polymer Composites*, Chapman & Hall.

Composites Part A: Applied Science and Manufacturing, Elsevier, Oxford, UK.

Polymer Composites, Society of Plastics Engineers (SPE), Brookfield, CT, USA.

Journal of Composite Materials, Technomic, Lancaster, PA, USA.

References

ADAMS, K. L., RUSSEL, W. B. & REBENFELD, L. (1988) Radial penetration of a viscous liquid into a planar anisotropic porous medium. *International Journal of Multiphase Flow,* 14**,** 203-215.

AMBROSI, D. & PREZIOSI, L. (1998) Modeling matrix injection through porous performs. *Composites, Part A,* 29**,** 5-18.

BOGETTI, T. A. & GILLESPIE, J. W., JR. (1991) Two-dimensional cure simulation of thick thermosetting composites. *Journal of Composite Materials,* 25**,** 239-273.

CAI, Z. (1992a) Analysis of mold filling in RTM process. *Journal of Composite Materials,* 26**,** 1310-1377.

CAI, Z. (1992b) Simplified mold filling simulation in resin transfer molding. *Journal of Composite Materials,* 26**,** 2606-2630.

CHANG, C. Y. & HOURNG, L. W. (1998) Study on void formation in resin transfer molding. *Polymer Engineering and Science,* 38**,** 809-818.

FARINA, A. & PREZIOSI, L. (2000) Non-isothermal injection molding with resin cure and perform deformability. *Composites, Part A,* 31**,** 1355-1372.

GAMA, B. A., LI, H., LI, W., PAESANO, A., HEIDER, D. & GILLESPIE, J. W., JR. (2001) Improvement of dimensional tolerances during VARTM processing. *33rd International SAMPE Technical Conference.* Seattle, WA, Society for the Advancement of Material and Process Engineering.

GONG, H. (1993) Pressure distribution in resin transfer molding with a non-rigid fiber perform. *Journal of Materials Processing Technology,* 37**,** 363-371.

GONZALEZ-ROMERO, V. M. & CASILLAS, N. (1989) Isothermal and temperature programmed kinetic studies of thermosets. *Polymer Engineering and Science,* 29**,** 295-301.

GOTOWSKY, T. G. (1997) *Advanced Composite Manufacturing*, John Wiley & Sons.

GUTOWSKI, T. G., WINEMAN, S. J. & CAI, Z. (1986) Applications of the resin flow/fiber deformation model. *Proceedings of the 33rd National SAMPE Symposium***,** 245-254.

HAMIDI, Y. K., AKTAS, L. AND ALTAN, M.C., (2004) Formation of microscopic voids in resin transfer molded composites. *ASME Transactions: Journal of Engineering Materials and Technology,* 126**,** 420-426.

HOLMBERG, J. A. & BERGLUND, L. A. (1997) Manufacturing and performance of RTM U-beams. *Composite Part A,* 28**,** 513-521.

JIANG, S., ZHANG, C. & WANG, B. (2002) Optimum arrangement of gate and vent locations for RTM process design using a mesh distance-based approach. *Composites Part A,* 33**,** 471-481.

KAMAL, M. R. (1974) Thermoset characterization for moldability analysis. *Polymer Engineering and Science,* 14**,** 231-239.

KAMAL, M. R. & SOUROUR, S. (1973) Kinetics and thermal characterization of thermoset cure. *Polymer Engineering and Science,* 13**,** 59-64.

KANG, M. K., LEE, W.I. AND HAHN, H.T. (2000) Formation of microvoids during resin-transfer molding process. *Composite Science and Technology,* 60**,** 2427-2434.

LEE, W. I., LOOS, A.C. AND SPRINGER, G.S. (1982) Heat of reaction, degree of cure, and viscosity of Hercules 3510-6 resin. *Journal of Composite Materials,* 16**,** 510-520.

LI, J., ZHANG, C., LIANG, R. & WANG, B. (2006) Modeling and analysis of thickness gradient and variation in VARTM processes. *SAMPE 2006.* Long

Beach, CA, Society for the Advancement of Material and Process Engineering.
LIU, B., BICKERTON, S. & ADVANI, S. G. (1996) Modeling and simulation of resin transfer molding (RTM) – gate control, venting and dry spot prediction. *Composites Part A,* 27**,** 135-141.
LOOS, A. C. & SPRINGER, G. S. (1983) Curing of epoxy matrix composites. *Journal of Composite Materials,* 17**,** 135-169.
LUCK, R. M. & SADHIR, R. K. (1992) Shrinkage in conventional monomers during polymerization. IN SADHIR, R. K. & LUCK, R. M. (Eds.) *Expanding Monomers.* Boca Raton, FL, CRC Press.
PARNAS, R. S., SALEM, A. J., SADIK, T. A. K., WANG, H. P. & ADVANI, S. G. (1994) The interaction between micro- and macro-scopic flow in RTM preforms. *Composite Structures,* 27**,** 93-107.
PATEL, N. & LEE, L. J. (1995) Effects of fiber mat architecture on void formation and removal in liquid composite molding. *Polymer Composites,* 16**,** 386-399.
PATEL, N., ROHATGI, V. AND LEE, L.J. (1995) Micro scale flow behavior and void formation mechanism during impregnation through a unidirectional stitched fiberglass mat. *Polymer Engineering and Science,* 35**,** 837-851.
ROBITAILLE, F. & GAUVIN, R. (1998) Compaction of textile reinforcements for composite manufacturing. II: Compaction and relaxation of dry and H2O saturated woven reinforcements. *Polymer Composites,* 19**,** 543-557.
ROBITAILLE, F. & GAUVIN, R. (1999) Compaction of textile reinforcement for composites manufacturing. III: Reorganization of the fiber network. *Polymer Composites,* 20**,** 48-61.
ROHATGI, V., PATAL, N. & LEE, J. L. (1996) Experimental investigations of flow-induced microvoids during impregnation of unidirectional stitched fiberglass mat. *Polymer Composites,* 17**,** 161-170.
RUDD, C. D., RICE, E. V., BULMER, L. J. & LONG, A. C. (1993) Process modelling and design for resin transfer moulding. *Plastics, Rubber and Composites Processing and Applications,* 20**,** 67-76.
SVANBERG, J. M. & HOLMBERG, J. A. (2001) An experimental investigation on mechanisms for manufacturing induced shape distortions in homogeneous and balanced laminates. *Composites Part A,* 32**,** 827-838.
TAKEDA, F., NISHIYAMA, S., HAYASHI, K., KOMORI, Y., SUGA, Y. & ASAHARA, N. (2005) Research in the application of the VARTM technique to the fabrication of primary aircraft composite structures. *Mitsubishi Heavy Industries, Ltd. Technical Review,* 42.
TREVINO, L., RUPEL, K., YOUNG, W. B., LIOU, M. J. & LEE, L. J. (1991) Analysis of resin injection molding in molds with replaced fiber mats. I: Permeability and compressibility measurements. *Polymer Composites,* 12**,** 20-29.
TROCHU, F., RUIZ, E., ACHIM, V. & SOUKANE, S. (2006) Advanced numerical simulation of liquid composite molding for process analysis and optimization. *Composites, Part A,* 37**,** 890-902.
TUCKER, C. L., III (1993) Fundamentals of computer modeling for polymer processing. IN ADVANI, S. G. (Ed.) *Flow Phenomena in Polymer Composite.* Woodhead Publishing Ltd.
YATES, B., MCCALLA, B. A., PHILLIPS, L. N., KINGSTON-LEE, D. M. & ROGERS, K. F. (1979) The thermal expansion of carbon fiber-reinforced

plastics. Part 5: the influence of matrix curing characteristics. *Journal of Material Science,* 14**,** 1207-1217.